



RESEARCH ARTICLE

10.1002/2017GC006886

Superweak asthenosphere in light of upper mantle seismic anisotropy

Thorsten W. Becker^{1,2} ¹Institute for Geophysics, Jackson School of Geosciences, The University of Texas at Austin, Austin, Texas, USA,²Department of Geological Sciences, Jackson School of Geosciences, The University of Texas at Austin, Austin, Texas, USA

Key Points:

- Azimuthal anisotropy sensitive to asthenospheric mechanical properties
- Suboceanic plate asthenosphere ~ 0.1 – 0.01 times upper mantle viscosity
- Isolated, superweak asthenosphere does not affect global dynamics

Correspondence to:

T. W. Becker,
twb@ig.utexas.edu

Citation:

Becker, T. W. (2017), Superweak asthenosphere in light of upper mantle seismic anisotropy, *Geochem. Geophys. Geosyst.*, 18, doi:10.1002/2017GC006886.

Received 23 FEB 2017

Accepted 20 APR 2017

Accepted article online 27 APR 2017

Abstract Earth's upper mantle includes a ~ 200 km thick asthenosphere underneath the plates where viscosity and seismic velocities are reduced compared to the background. This zone of weakness matters for plate dynamics and may be required for the generation of plate tectonics itself. However, recent seismological and electromagnetic studies indicate strong heterogeneity in thinner layers underneath the plates which, if related to more extreme, global viscosity reductions, may require a revision of our understanding of mantle convection. Here, I use dynamically consistent mantle flow modeling and the constraints provided by azimuthal seismic anisotropy as well as plate motions to explore the effect of a range of global and local viscosity reductions. The fit between mantle flow model predictions and observations of seismic anisotropy is highly sensitive to radial and lateral viscosity variations. I show that moderate suboceanic viscosity reductions, to ~ 0.01 – 0.1 times the upper mantle viscosity, are preferred by the fit to anisotropy and global plate motions, depending on layer thickness. Lower viscosities degrade the fit to azimuthal anisotropy. Localized patches of viscosity reduction, or layers of subducted asthenosphere, however, have only limited additional effects on anisotropy or plate velocities. This indicates that it is unlikely that regional observations of subplate anomalies are both continuous and indicative of dramatic viscosity reduction. Locally, such weak patches may exist and would be detectable by regional anisotropy analysis, for example. However, large-scale plate dynamics are most likely governed by broad continent-ocean asthenospheric viscosity contrasts rather than a thin, possibly high melt fraction layer.

1. Introduction

Plate tectonics is the surface expression of mantle convection, and the plates themselves can be defined as being part of the cold, upper thermal boundary layer of convection cells. Relatively cold temperatures lead to high viscosities in the uppermost ~ 100 km of the mantle, the lithosphere. The underlying mantle is hotter, and hence weaker, and any such weak substratum can be called the asthenosphere. However, typically "asthenosphere" refers to a particularly weak zone, relative to the rest of the upper mantle, between ~ 100 and ~ 300 km depth. In this depth range, horizontally averaged seismic wave velocities are reduced compared to the steady, adiabatic increase with depth [Gutenberg, 1959].

There are a range of explanations for the seismological observation of an asthenospheric low velocity zone, partial melt, and increased volatile contents among them [e.g., *Stixrude and Lithgow-Bertelloni*, 2005; *Hirschmann*, 2010]. However, nonadiabatic temperatures may also be the cause [Jeanloz and Morris, 1987]. This would be expected from the overshoot observed underneath the top boundary layer in high Rayleigh number convection [Gurnis and Davies, 1986; Jarvis and Peltier, 1989], particularly in a plume-fed asthenosphere scenario [Phipps Morgan et al., 1995], and/or for the predominance of internal heating [Olson, 1981; Gurnis and Davies, 1986]. All these velocity reduction mechanisms are also expected to lead to a reduction of viscosity, as required for a mechanically defined asthenosphere. Yet, none of these mechanisms are required for a viscosity reduction in the relevant depth range because the activation volume and energy of olivine leads to a low viscosity zone based on adiabatic temperature and pressure increase with depth alone [Hirth and Kohlstedt, 2004; Podolefsky et al., 2004; Billen and Hirth, 2005; Becker, 2006].

Constraints from geoid and postglacial rebound modeling as well as laboratory creep laws appear consistent with roughly ~ 2 order of magnitude reduction of viscosity compared to the upper mantle in the depth range between ~ 100 and ~ 300 km [Hirth and Kohlstedt, 2004]. Mantle convection and plate tectonics are

therefore likely associated with a ~ 200 km thick, moderately low viscosity zone underneath the plates. Such a “regular” asthenospheric layer may indeed be required for the formation of the plate tectonic regime of surface motions [Tackley, 2000; Richards *et al.*, 2001; Lenardic *et al.*, 2006; Hoink and Lenardic, 2008; van Heck and Tackley, 2008; Foley and Becker, 2009]. However, a range of recent observations call our general understanding of the mechanics of plate motion generation into question and suggest a “superweak” asthenosphere, with more extreme viscosity reduction in a possibly thinner layer.

For example, Kawakatsu *et al.* [2009] suggested that impedance contrasts imaged seismologically in oceanic mantle at the inferred base of the lithosphere may be indicative of a thin, high partial-melt fraction layer. Consistent with such a suggestion, Naif *et al.* [2013] found an anisotropic, high electric conductivity layer underneath the Cocos plate in the vicinity of the trench, and Hawley *et al.* [2016] argued for melt accumulation underneath the Cascadia slab based on seismic tomography. Moreover, Stern *et al.* [2015] documented a strong seismic reflector at the base of the Pacific plate, interpreted as a decoupling layer. Those studies mainly speak to structural heterogeneity and constrain mechanical behavior only in indirect ways such as inferred melt content. The ~ 4 orders of magnitude viscosity reduction based on partial melt suggested by Stern *et al.* [2015], for example, appears to be at the high end of typical estimates. However, ~ 2 orders of magnitude melt-induced viscosity drops might still be expected even from small partial melt fractions, with complications due effects of contiguity, as discussed by Holtzman [2016].

Recently, large earthquakes in well-instrumented settings have allowed geodesy-based inferences on sub-oceanic plate asthenospheric viscosities for the first time. Hu *et al.* [2016] modeled postseismic deformation after the 2012 Indian Ocean earthquake and inferred a ~ 0.05 drop of viscosity for a ~ 100 km thick asthenospheric layer compared to the upper mantle reference. Freed *et al.* [2017] detected a more localized, low viscosity zone in the bottom of the subducting Pacific plate based on postseismic deformation after the 2011 Tohoku-oki earthquake. This basal weak zone could be either fairly broad with moderate viscosity reduction compared to the upper mantle, as expected based on where the slab might experience Peierls plasticity [Buffett and Becker, 2012], or the weak layer could be thin and even lower viscosity as might be expected based on the suggested decoupling layer of Stern *et al.* [2015] [Freed *et al.*, 2017]. Having superweak layers underneath the plates may well affect plate driving forces and transmission of mantle-flow induced tractions.

Given these intriguing observations and remaining uncertainties about the nature of the lithosphere-asthenosphere transition even in oceanic lithosphere [e.g., Burgos *et al.*, 2014; Beghein *et al.*, 2014; Auer *et al.*, 2015; Holtzman, 2016; Hansen *et al.*, 2016], it seems useful to seek to further constrain the dynamics of the asthenosphere. In particular, it may be of interest to evaluate new kinds of asthenosphere models in light of their predictions for plate driving forces and other constraints such as the gravitational geopotential. However, those two constraints are notoriously nonunique. Nonhydrostatic geoid anomalies, for example, indicate a preference for mantle flow to be subjected to an asthenospheric viscosity reduction [Hager, 1984], but the geoid can be fit with a range of radial viscosity profiles [King, 1995; Panasyuk and Hager, 2000; Mitrovica and Forte, 2004; Paulson *et al.*, 2005]. Considering plate motions, one important metric is the partitioning of plate speeds, where oceanic lithosphere typically moves faster than continental lithosphere. However, this can be explained by the relative weakness of the asthenosphere under the oceanic plates [Ricard *et al.*, 1991; Zhong, 2001; Becker, 2006], predominantly one-sided slab pull [Forsyth and Uyeda, 1975; Conrad and Lithgow-Bertelloni, 2002], or, quite likely, a combination of the two [van Summeren *et al.*, 2012; Alisic *et al.*, 2012].

A different set of constraints is therefore welcome, and may be provided by seismic anisotropy. If caused by the lattice-preferred orientation (LPO) of intrinsically anisotropic minerals such as olivine, as is commonly assumed for the upper mantle [e.g., Silver, 1996; Long and Becker, 2010], anisotropy is sensitive to progressive shear of rocks under convection. Particularly azimuthal anisotropy as inferred from surface waves can be related to mantle flow in a fairly straightforward way [McKenzie, 1979; Tanimoto and Anderson, 1984; Montagner and Tanimoto, 1991]. An argument has been made that mantle flow computations predict more physically realistic misfits with seismological observations than simple alignment with uniform shear as assumed from surface plate motions alone [Becker *et al.*, 2014]. Moreover, Becker *et al.* [2003] showed that the fit between mantle flow model predictions and azimuthal anisotropy is sensitive to radial variations in viscosity. For example, a strong viscosity reduction at 660 km depth led to a dramatic increase in misfit between mantle flow model predictions and anisotropy. This sensitivity of seismic anisotropy to shear was

exploited by *Becker* [2008] and *Conrad and Behn* [2010] to constrain the largest-scale shear possible, the amount of net rotation of the surface of the Earth to the deep mantle, for example. These findings also suggest that azimuthal anisotropy can be further probed to understand the range of more complex asthenospheric viscosity reduction scenarios that are consistent with our current understanding of plate tectonics.

Here, I explore a large number of global mantle circulation models with a range of lateral viscosity variations within the oceanic upper mantle, designed to test the effect of superweak asthenospheric channels and patches on seismic anisotropy and plate motion predictions.

2. Methods

My global mantle flow computations consider mantle circulation as driven by internal density sources and the resulting plate motions [*Hager and O'Connell*, 1981; *Hager*, 1984; *Ricard and Vigny*, 1989]. Models are based on the approach of *Miller and Becker* [2012], where a range of density models as inferred from Wadati-Benioff zone seismicity and conversion of seismic tomography were explored. Combined with assumptions on mantle viscosity variations, in particular the presence of predefined weak zones along plate boundaries, such dynamically consistent models of plate tectonics are able to match observed plate motions and the nonhydrostatic geoid fairly well [*Zhong et al.*, 2000; *Ghosh et al.*, 2010]. My reference model has four broad mechanical layers of lithosphere, asthenosphere, as well as upper and lower mantle, and achieves correlation with plate motions of 0.92 while matching geoid anomalies at a 0.75 correlation level. This is typical for the best such models [*Ghosh et al.*, 2010].

Further model optimization, e.g., by means of introduction of a larger number of viscosity layers, could presumably improve the match to the geoid. However, my chosen approach here is to start from a relatively simple, moderately well-performing model that includes a mix of upper mantle slabs, low velocity anomalies from upper mantle seismic tomography, and lower mantle seismic tomography as well as lateral viscosity variations very similar to the best-fit model of *Miller and Becker* [2012], see their supporting information Figure S2. I will then test how the mantle flow predictions are modified if the oceanic asthenosphere has additional local or regional viscosity reductions. While the starting model may not be “perfect,” I will assume that the variations from it will be general enough so as to apply even if the details of plate driving force transmission may be different in reality.

I employ Newtonian, temperature-dependent rheologies with further lateral variations in viscosity as inferred from the geological setting [*Ghosh et al.*, 2010; *Miller and Becker*, 2012]. The reference model has a global average viscosity that changes from $\approx 350\eta_0$ in the top 100 km, to $\approx 0.3\eta_0$ in the 100–300 km range, to η_0 in the remainder of the upper mantle, and $150\eta_0$ below 660 km, with a nominal upper mantle reference viscosity of $\eta_0 = 10^{21}$ Pas. Subcontinental regions are stronger than suboceanic ones, with the viscosities in the background asthenosphere between 100 and 300 km averaging to $\approx 3\eta_0$ and $\approx 0.07\eta_0$, respectively, because of the effects of temperature-dependence and prescribed cratonic keels [cf., *Miller and Becker*, 2012].

As for the viscosity variations tested, Figure 1a shows the reference model viscosity at ≈ 135 km depth, just underneath the high viscosity lithosphere. From this reference, I explore variations of the viscosity prefactors where

1. the background asthenospheric viscosity within the 100–300 km depth range underneath oceanic plates is reduced uniformly;
2. the viscosity reduction applies underneath the oceanic lithosphere, but only in a narrower, 100–150 km range, as might be expected if the layer detected locally by *Kawakatsu et al.* [2009] and *Stern et al.* [2015], for example, would have an effect on rheology and be global (Figure 1b);
3. the thin suboceanic plate layer of 2) gets subducted behind slabs (defined based on the RUM model by *Gudmundsson and Sambridge* [1998]) as suggested by *Song and Kawakatsu* [2012] based on anisotropy in subduction zones and modeled regionally in two-dimensions by *Liu and Zhou* [2015];
4. the thin, 50 km thickness viscosity reduction only applies close to subduction zones (Figure 1c), where most observations are located [cf., *Naif et al.*, 2013; *Hawley et al.*, 2016];
5. there are two stripes of viscosity reduction, perhaps due to melt accumulation at ridges and at subduction zones (Figure 1d);

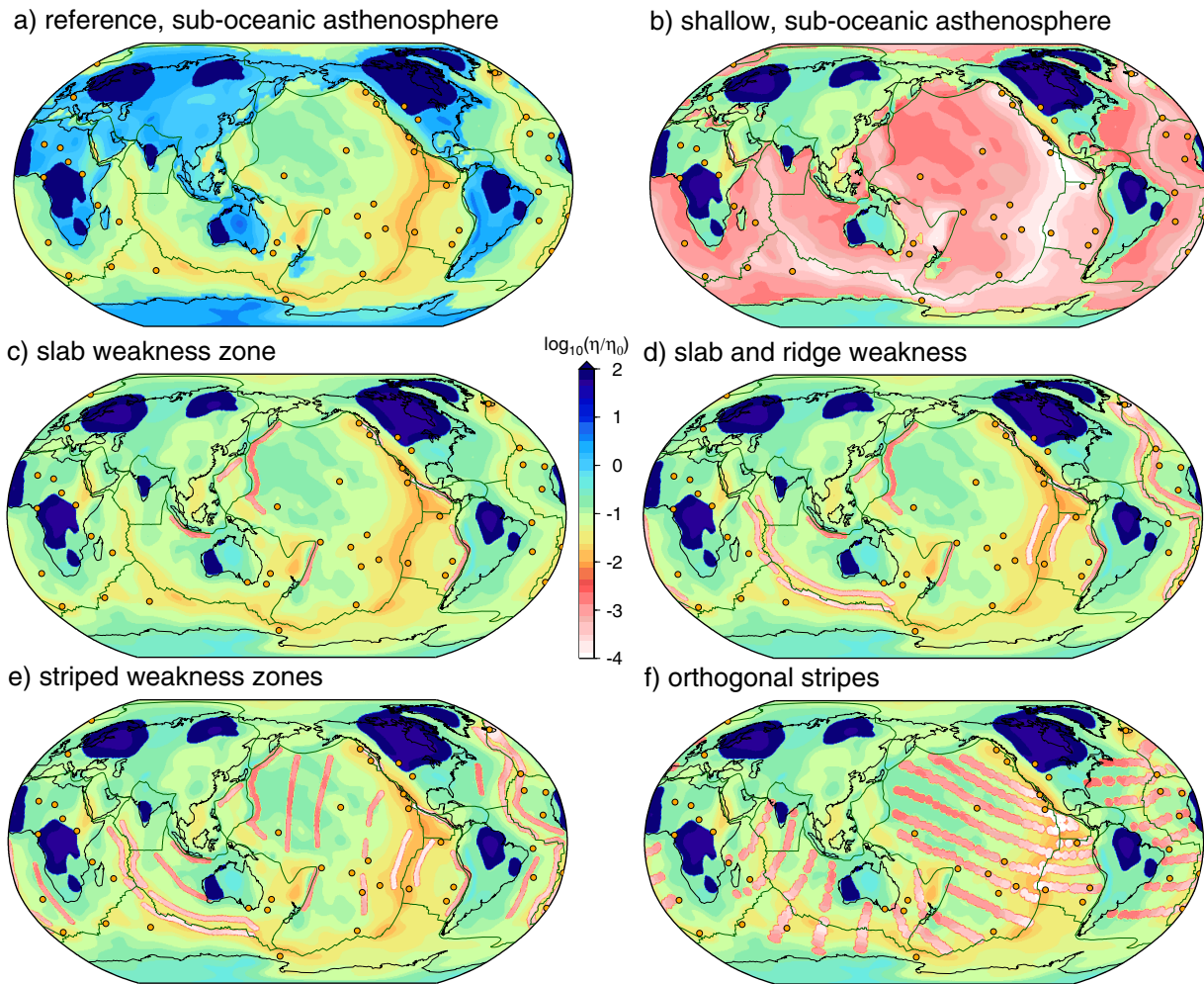


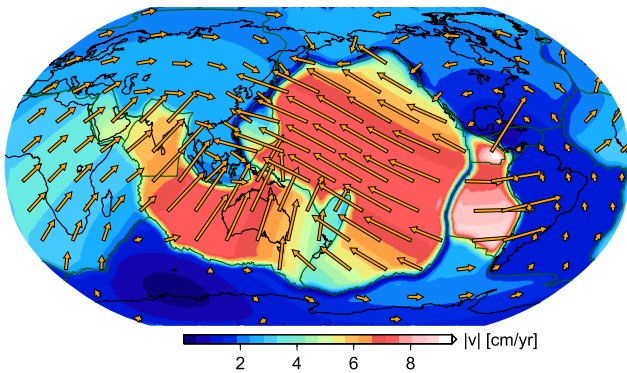
Figure 1. Example viscosity models at ≈ 135 km depth. (a) Reference model, including the effect of temperature-dependence given tomographically inferred variations in the upper mantle plus slabs as well as geologically/structurally motivated variations such as continental keels [Ghosh *et al.*, 2010; Miller and Becker, 2012] and weak zones (in the upper 100 km, not shown). Suboceanic-plate, background viscosity between 100 and 300 km is reduced to $\eta_a = 0.1\eta_0$, where η_0 is the reference upper mantle. (b) Suboceanic viscosity is reduced between 100 and 150 km to $\eta_a = 0.01\eta_0$, and the global background viscosity between 100 and 300 km is $0.1\eta_0$ for this and all subsequent models. (c) Subduction zone local η_a viscosity reduction; (d) subduction zones and ridges underlain by weakened asthenosphere; (e) several stripes; and (f), orthogonal stripes of asthenospheric weakness. Weakness zones in Figures 1c–1f are ad hoc to explore general effects, rather than match regional details. Orange dots are major hotspots for reference.

6. there are several weak asthenosphere stripes to test the effects of increasing the coherence of viscosity reduction (Figure 1e); and, last,
7. stripes that are broadly aligned with plate motions, as if Richter [1973] rolls were to lead to viscosity reduction (Figure 1f).

Mantle circulation is estimated using the well-benchmarked finite element software CitcomS [Moresi and Solomatov, 1995; Zhong *et al.*, 2000] that solves the conservation equations for momentum and mass (instantaneous Stokes solution) under the Boussinesq and infinite Prandtl number assumptions. Parameter choices are generally as in Miller and Becker [2012], but I apply a higher numerical resolution to resolve spatially localized lateral viscosity variations. Horizontally, the model has $193 \times 193 \times 12$ nodes in a layer (~ 17 km global, average resolution), and 193 nodes subdivide the mantle radially, leading to 84,934,656 elements in total. Vertical node spacing is reduced in the upper mantle, down to ~ 7 km in the top 400 km.

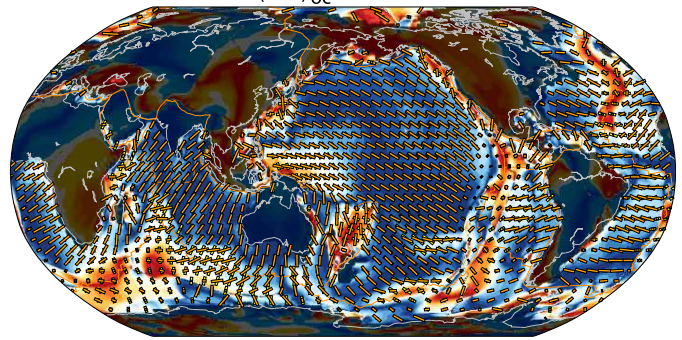
This resolution allows capturing the narrow, asthenosphere features of concern (Figure 1), such that at least ≥ 7 elements are found in each layer with depth. I iterate on the initial Stokes solution to ensure the Uzawa iterations [Moresi and Solomatov, 1995] are truly converged. I also tested the robustness of results compared with lower resolution meshes and found that conclusions remain unchanged even for the coarser resolution used in Miller and Becker [2012] (~ 11 km vertically in the surface layers), and doubling local vertical

a) surface velocities, prescribed plate motions



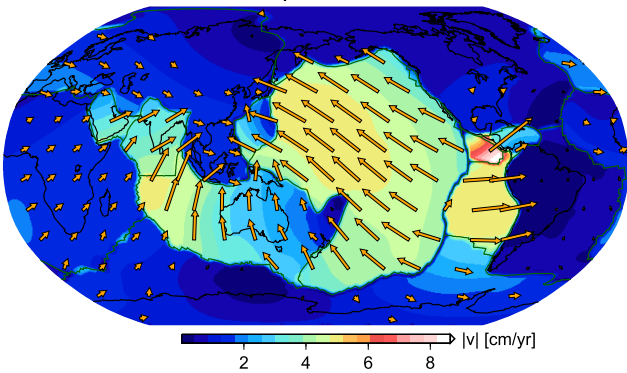
b) anisotropy misfit for model a)

$$\langle \Delta\alpha \rangle_{oc} = 26.0^\circ$$



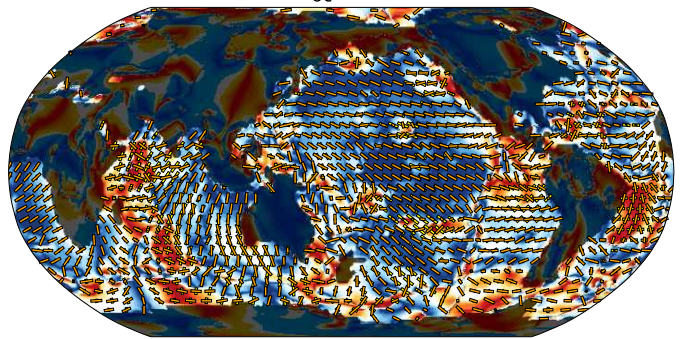
c) surface velocities, slabs and upper mantle anomalies

$$r_v = 0.916$$



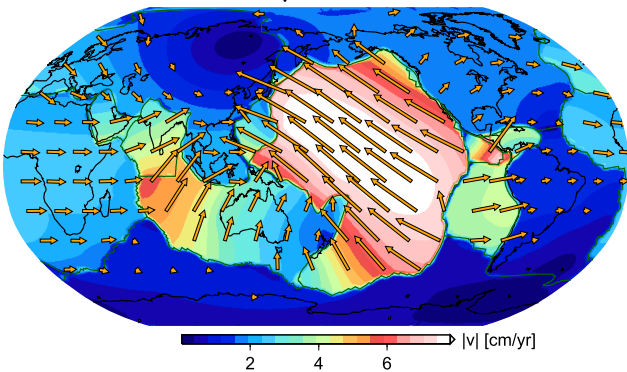
d) anisotropy misfit for model c)

$$\langle \Delta\alpha \rangle_{oc} = 32.9^\circ$$



e) surface velocities, slabs, upper mantle, low viscosity

$$r_v = 0.910$$



f) anisotropy misfit for model e)

$$\langle \Delta\alpha \rangle_{oc} = 42.2^\circ$$

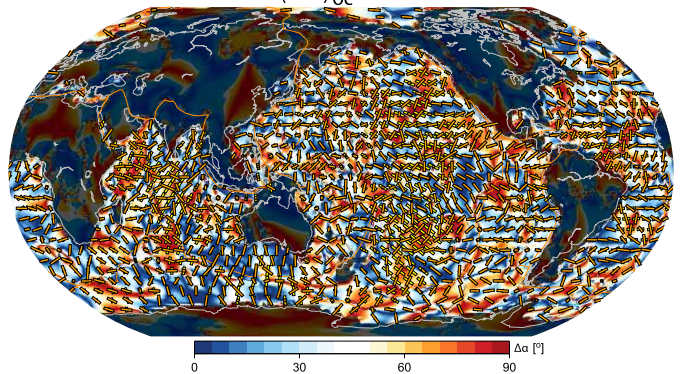


Figure 2. (left) Surface velocities as (a) prescribed and (c, e) predicted; (right; b, d, f) match of inferred seismic anisotropy with azimuthally anisotropic SV tomography [Schaeffer *et al.*, 2016] at 200 km depth. Velocities are indicated by orange vectors with magnitude as background shading (variable scale). r_v denotes the correlation of predictions with observations. For anisotropy, orange sticks are fast polarization orientations from tomography, yellow inferred from the flow model. Background shading indicates angular misfit, $\Delta\alpha$; average misfit in the bright, oceanic regions, $\langle \Delta\alpha \rangle_{oc}$, shown in title for each model. Plots a and b are from the model of Becker *et al.* [2008] as used in Becker *et al.* [2014]; plot c/d is my dynamically consistent reference model with slab and tomography-inferred density anomalies (cf. Figure 1a); and e/f use the same density structure as plot c/d but an oceanic viscosity that is reduced by a factor of 0.01 compared to c/d.

resolution also indicates convergence of flow estimates. Viscosity variations are limited to the range of $[10^{-4}; 10^4]$ relative to the background mantle viscosity, η_0 , though locally viscosity typically changes by \leq four orders of magnitude on relevant scales (Figure 2).

Tomographic shear wave velocity anomalies, $d \ln v_s = \Delta v_s / \langle v_s \rangle$, are scaled to density, ρ , according to $d \ln \rho / d \ln v_s = 0.2$ [Ghosh *et al.*, 2010]. A total of 101 global mantle flow computations were considered, with viscosity parameters varied as illustrated in Figure 1. To isolate the role of upper mantle slabs pulling the plates as

opposed to a combination of buoyant upwellings and slabs, I will also show results where contributions from the upper mantle outside Wadati-Benioff zones are ignored [cf., *Becker and O'Connell*, 2001; *Conrad and Lithgow-Bertelloni*, 2002; *Ghosh et al.*, 2010; *Alisic et al.*, 2012].

In the case of buoyancy driven flow, velocity amplitudes depend on the ratio of density anomalies and viscosity. Density anomalies in mantle circulation models are somewhat uncertain, for reasons including the possibly inaccurate representation of anomaly amplitudes by tomography, complexities of the mineral physics relationships as a function of temperature, pressure, and phase, and other effects of compositional heterogeneity [e.g., *Forte et al.*, 2015]. Slab-only tests can therefore provide some insights into the slab-pull related, plate-scale flow independent of mantle density anomalies outside subduction zones [cf., *Hager*, 1984]. Those models are not meant to be complete representations of plate driving forces but rather to illustrate the flow contribution of the slab pull component.

Once mantle circulation is estimated, I then compute global, synthetic seismic anisotropy for each flow model, following the approach of *Becker et al.* [2006]. For each point of observation, this involves backtracking the flow path which transports material to the point where anisotropy is supposed to be estimated such that, starting from zero deformation, a critical, logarithmic finite strain, ξ , is reached. LPOs are then computed from the velocity gradient matrix along the forward flow paths using the method of *Kaminski et al.* [2004] for the regular (dry and low-stress) "A type" of olivine LPO. The idea is that this strain will be sufficient to overprint any existing LPO. For each layer, $\sim 14,500$ roughly equal-area distributed points are estimated, and layers are placed in 20 km intervals from 20 to 380 km depth. I use a critical finite strain of $\xi=0.75$ as in *Becker et al.* [2014] but conclusions are the same for larger overprinting strains such as $\xi=1.5$ because ξ controls mainly the magnitude rather than orientation of LPOs [*Becker et al.*, 2006]. Since $\xi=0.75$ saturation strains are typically reached in less than ~ 10 Myr [*Becker et al.*, 2006], and earlier tests did not yield an improvement in the fit to surface wave models [*Becker et al.*, 2003], I do not consider time-dependent flow here for simplicity.

LPO anisotropy is expected to form predominantly under dislocation creep, and the best-fit model used in *Becker et al.* [2014] employs the effective dislocation-diffusion creep rheology and approach of *Becker et al.* [2008] to account for such complexities. Here, I employ only Newtonian flow models, for simplicity, and have LPO develop everywhere in the upper 400 km of the mantle. Differences in mantle flow directions between Newtonian and non-Newtonian models are moderate on global scales [*Becker*, 2006], such that the Newtonian simplification is expected to affect the depth distribution of anisotropy strength more than the "fast axes" (i.e., azimuth of fast v_{SV} polarization orientations). The latter are estimated by assigning elastic constants to the synthetic LPOs and extracting the relevant elastic tensor components for comparison with azimuthal anisotropy tomography [*Becker et al.*, 2007], and then computing a local angular misfit, $\Delta\alpha \in [0^\circ; 90^\circ]$.

There are, of course, several uncertainties and simplifications in any computation of synthetic seismic anisotropy. Here, these include the neglect of time-dependent flow and power law behavior and uncertainties as to the type or micromechanics of LPO formation [*Becker et al.*, 2008; *Castelnau et al.*, 2009]. However, the azimuthal anisotropy that is estimated in simplified ways does lead to a good fit to observations when compared to global tomographic estimates [*Becker et al.*, 2003, 2014] or regional shear-wave splitting measurements [*Miller and Becker*, 2012]. This gives me confidence that this approach provides a meaningful link between the time-integrated effects of mantle flow as modulated by the asthenosphere and the diagnostic set of anisotropy observations [*Gaboret et al.*, 2003; *Becker et al.*, 2003; *Behn et al.*, 2004; *Conrad and Behn*, 2010].

3. Results

3.1. Example Models

Figure 2 shows surface velocities and asthenospheric (200 km depth) match of flow model predictions of LPOs to azimuthal seismic anisotropy from the tomographic model by *Schaeffer et al.* [2016]. For reference, Figure 2a shows a smoothed version of NUVEL1A-NNR [*DeMets et al.*, 1994] plate model velocities which were prescribed as a surface boundary conditions for the radial anisotropy tests of *Becker et al.* [2008]. The best-fit flow model from that study included a diffusion-dislocation creep composite rheology at constant grain size [*Becker*, 2006] and had LPO form only in the dislocation creep dominated regions. *Becker et al.*

[2014] used this older LPO model for consistency to compare with newer seismological estimates, and fits such as that in Figure 2b were compared by Becker et al. with those based on alignment with absolute plate motions [Debayle and Ricard, 2013; Burgos et al., 2014].

In the following, I will focus my discussion of asthenospheric seismic anisotropy on suboceanic domains deeper than ~ 100 km. Those are expected to more readily reflect present-day convective flow. In contrast, shallower, oceanic plate regions, or continental lithosphere may be both compositionally more heterogeneous and dominated by a frozen-in record of plate formation or past deformation [e.g., Silver, 1996; Debayle and Ricard, 2013; Becker et al., 2008, 2014; Auer et al., 2015]. Suboceanic azimuthal anisotropy in the asthenosphere is indeed generally better matched by mantle flow models than continental regions [Becker et al., 2007; Debayle and Ricard, 2013].

Figures 2c and 2d show the surface velocity predictions and asthenospheric match to azimuthal anisotropy, respectively, for my reference, dynamically consistent mantle flow model. The correlation of plate motions with the observations is fairly good at the 0.916 level, as noted, though improvements could likely be achieved by adjusting the density or viscosity structure [cf., Becker and O'Connell, 2001; Aliscic et al., 2012; Forte et al., 2015]. The match of the LPO inferred from the dynamically consistent model to seismic anisotropy is somewhat worse (increase of average, angular misfit in oceanic plate regions, $\langle \Delta\alpha \rangle_{oc}$, of 7°) compared to the prescribed plate motion model of Becker et al. [2008] (Figure 2b). However, most oceanic regions are still well predicted by this flow model, with the exception of parts of the south Atlantic and Indian Ocean.

Untangling the origin of these discrepancies would mean having to achieve an even better fit of the flow models to plate motions which is beyond the scope or focus of this study. However, it appears that the balance between the enforced, plate-scale motions of Figures 2a and 2b, and the consistent flow of Figures 2c and 2d leads to more smaller-scale structure underneath the oceanic plates for the self-consistent models, such as the local disruption of anisotropic patterns around the Hawaiian hotspot in Figure 2d. This disruption may be real and not imaged by the large-scale anisotropic tomography [cf., Walker et al., 2005], or an artifact of giving too much weight to the density anomalies from tomography. In contrast, the large subspreading center mismatch of the prescribed plate motion model of Becker et al. [2008] (Figure 2b) is less pronounced when plate motions result self-consistently.

Regardless of those interesting details which may serve for further model refinement, e.g., in terms of treatment of LPOs, I take the results of the self-consistent computations such as in Figure 2d to yield an adequate fit to azimuthal anisotropy observations for most of the oceanic regions that warrants further tests. The following discussions of flow model match to azimuthal anisotropy are therefore based on these new, self-consistent flow models alone so as to be able to examine plate velocity predictions alongside seismic anisotropy.

For example, if I decrease the background, suboceanic asthenosphere viscosity between 100 and 300 km from $\eta_a = 0.1\eta_0$ of the reference model (Figures 2c and 2d) to $\eta_a = 0.001\eta_0$ (Figures 2e and 2f), the correlation with plate motions drops slightly, and the balance between the absolute oceanic and continental plate velocities is further shifted [Becker, 2006]. However, more dramatically, the match to anisotropy underneath oceanic plates at 200 km depth is disrupted almost everywhere by small-scale flow; $\langle \Delta\alpha \rangle_{oc}$ drops by $\approx 10^\circ$ to near random ($\langle \Delta\alpha \rangle = 45^\circ$) alignment. This indicates that azimuthal anisotropy is indeed quite sensitive to the shallow asthenosphere.

This decorrelation between LPO from flow model predictions and tomography as a function of η_a as seen in Figure 2f is not limited to single layer depths. Figure 3a shows the oceanic domain misfit with azimuthal anisotropy with depth when the 100–300 km depth asthenospheric viscosity is varied from the $\eta_a = 0.1$ reference model shown in Figure 2d. Besides the physical effects of interest that are related to the modified shearing in mantle flow, the misfit in such comparisons will be affected by several factors including depth-dependent resolution in the anisotropic tomography models [e.g., Becker et al., 2007] and the partitioning between dislocation and diffusion creep [Becker et al., 2008]. I do not attempt to correct for those effects here, but the misfit minimum at depths below the cold thermal boundary is consistent with earlier work [Debayle and Ricard, 2013; Burgos et al., 2014; Becker et al., 2008, 2014].

Overall, the reference viscosity model ($\eta_a = 0.1$) leads the lowest misfit with azimuthal anisotropy throughout most depths (Figure 3a). This is of note since that flow model was selected based on the match to plate velocities, the geoid, and regional seismic anisotropy originally [Miller and Becker, 2012], and not global

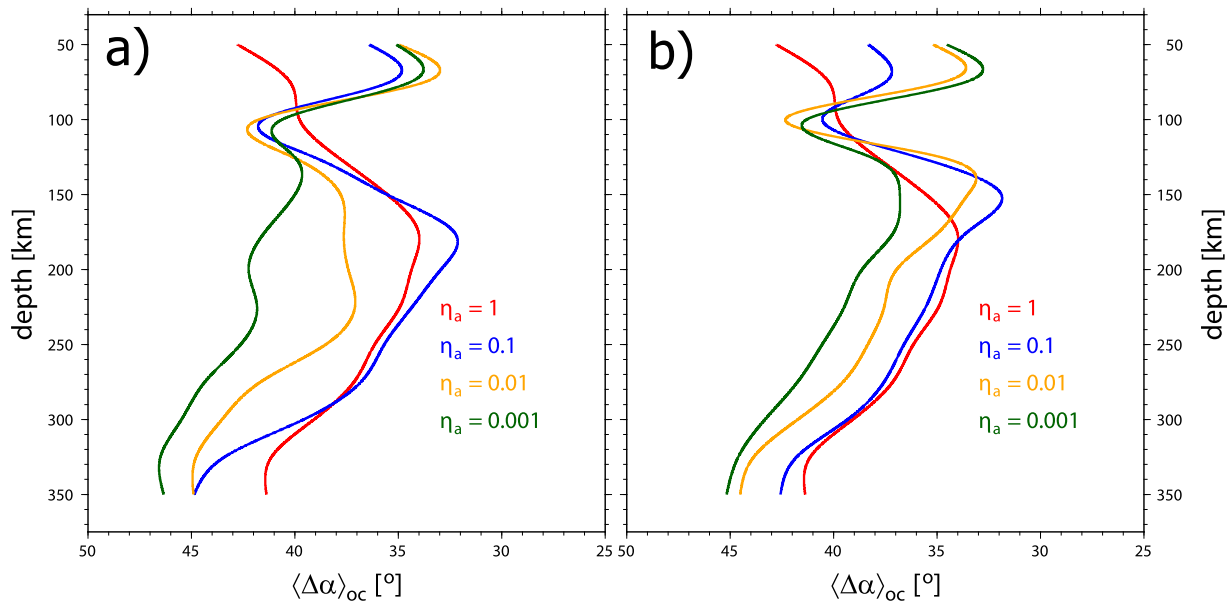


Figure 3. Mean angular misfit of azimuthal anisotropy from mantle flow models underneath oceanic plates, $\langle \Delta\alpha \rangle_{oc}$, when compared to the model of *Schaeffer et al.* [2016]. (a) Asthenospheric viscosity, η_a , is reduced between 100 and 300 km (reference model in Figures 2e and 2f has $\eta_a=0.1$). (b) Weak asthenosphere is limited to 100–150 km depth range.

anisotropy. The sublithospheric misfit minimum at ≈ 175 km is diminished when $\eta_a \leq 0.1$, and the lowest viscosities considered, $\eta_a = 0.001$, lead to angular misfits with anisotropy that are degraded to close to random levels in most regions underneath the lithosphere.

If the asthenospheric viscosity reduction underneath oceanic plates is limited to a thinner layer from 100 km to 150 km (Figure 3b), a similar degradation of fit to azimuthal anisotropy is seen for $\eta_a \leq 0.1$. The depth-integrated dependence of misfit on η_a is somewhat reduced, and the lowest misfit depth is shifted upward, localizing closer to the base of the mechanical lithosphere [cf., *Becker et al.*, 2014].

3.2. Mechanics of Flow Disruption

What causes the disruption of the asthenospheric shear that is apparently needed to have LPO induced by mantle flow explain azimuthal anisotropy? Inspection of the velocity fields themselves used to compute LPOs can serve to illustrate some of the effects. The velocity profile shown Figure 4 goes from the East Pacific Rise to the Japan subduction zone to capture the fairly simple convection system in the upper mantle underneath the Pacific plate. The profile is offset slightly to also capture the Hawaiian plume anomaly (cf. Figure 2d).

The reference model of Figure 4b ($\eta_a = 0.1$) shows mainly Couette (i.e., simple-shear) type flow underneath most of Pacific plate [cf., *Hoink and Lenardic*, 2010] besides toward the Nazca plate [cf., *Long and Becker*, 2010; *Natarov and Conrad*, 2012] and around the Hawaiian slow velocity anomaly (contour at $x \sim -1500$ km, also see Figure 4a) where a Poiseuille (i.e., pressure driven) character flow is found. The partitioning of flow into Couette and Poiseuille components was shown to be potentially detectable in seismic anisotropy if their flow directions are not aligned [*Natarov and Conrad*, 2012], though the depth resolution of anisotropic tomography puts some limitations on this in practice, particularly if the weakening layer is itself thinner than ~ 200 km.

The lower viscosity asthenosphere case of Figure 4c emphasizes how the flow is modified by a broad decoupling layer (cf. Figure 2f). Low η_a leads to strong vertical deflections around density anomalies, and extremely large asthenospheric velocities, several times the plate velocities. If the layer is thinner at the same viscosity reduction (Figure 4c), flow is channelled in a similar fashion, but the vertical deflections of flow below the weak asthenosphere are reduced to comparable levels to the reference model (Figure 4b). This appears consistent with the suggestion that an even thinner layer would display some channelized, Poiseuille flow compared to the reference but have a modest impact on deeper shear. Allowing for

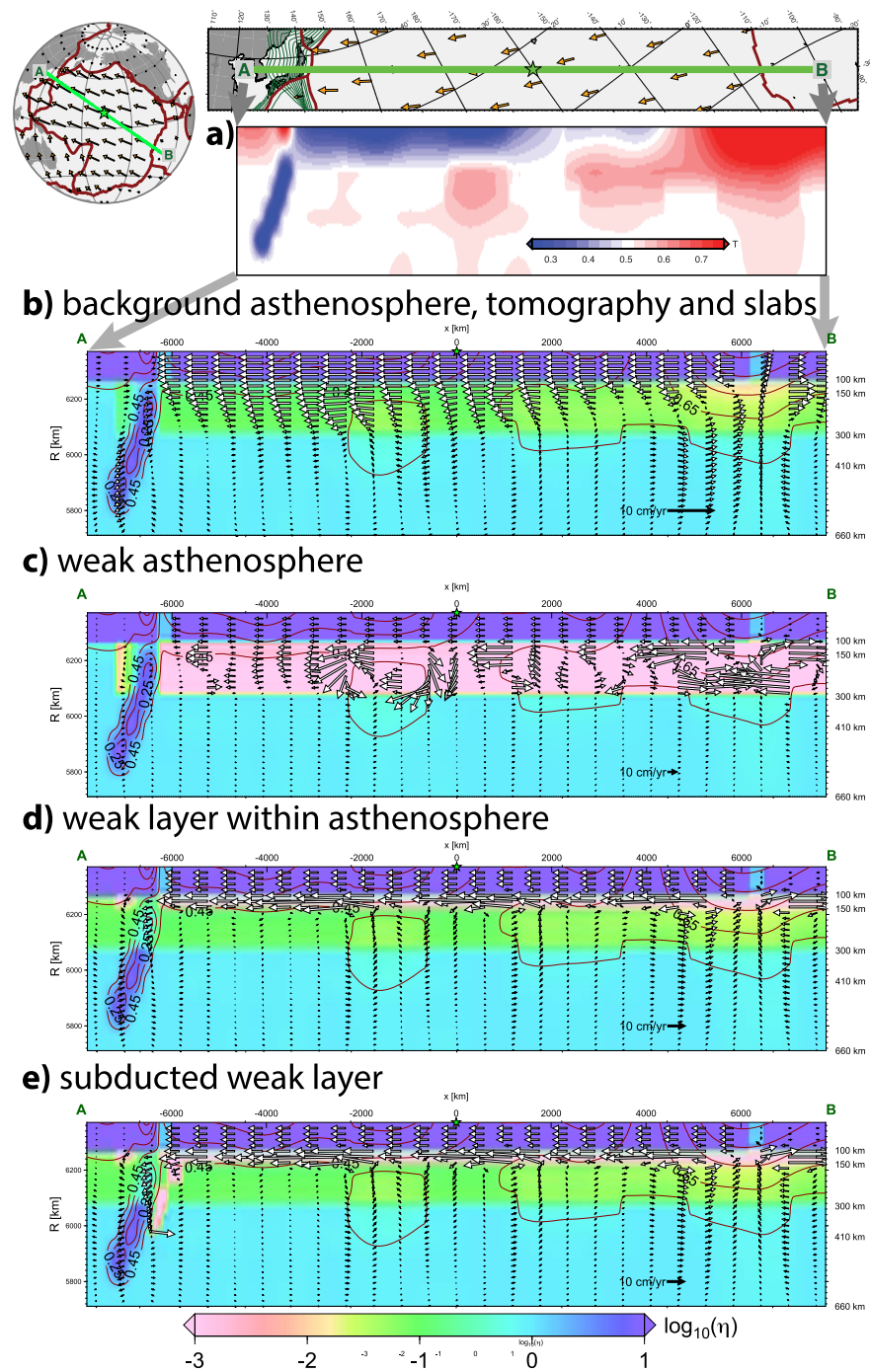
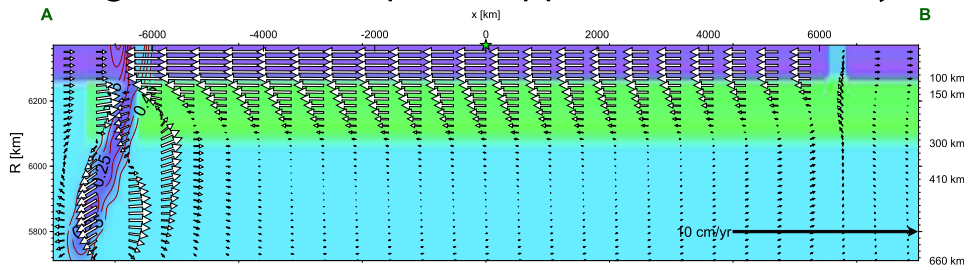


Figure 4. (a) Profiles for global mantle flow models using slabs and tomography, nondimensional temperature, T' . Background in Figures b–e is viscosity ($\eta = 1$ corresponding to reference, 10^{21} Pas), overlain by T' contours, and vectors denote flow velocities (variable scale). (b) Reference model (cf. Figures 2c and 2d); (c) reducing the viscosity in the suboceanic mantle as in Figures 2e and 2f; (d) limiting the similarly reduced viscosity channel to 100–150 km depth only; and (e), assuming that the low-viscosity channel is continued downward into the mantle. (top) hemispheric and oblique Mercator maps for profile location, surface velocities, plate boundaries, and slab contours (green lines) [from Gudmundsson and Sambridge, 1998].

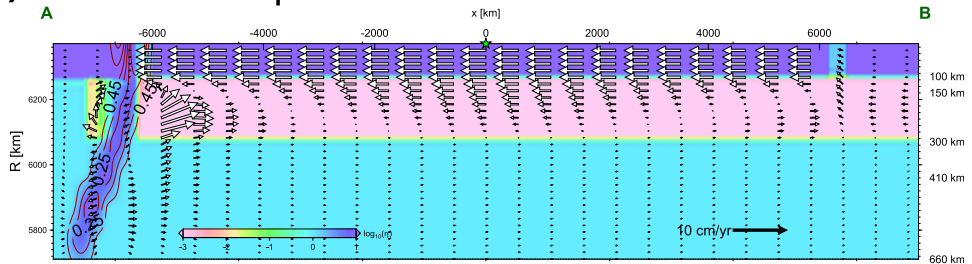
subduction of the thin asthenospheric layer (Figure 4e) does not modify plate velocities or mantle flow significantly further for my choices of parameterizing such a layer.

If we ignore any tomography-inferred density anomalies underneath the plates to explore model sensitivity, and only consider the component due to slab-pull induced, large-scale flow, the flow fields shown in Figure 5 result. The reference viscosity structure for slab-driven flow (Figure 5a) yields general plate-scale shear

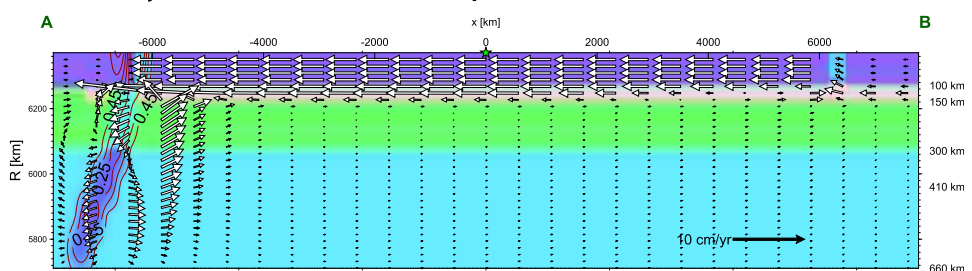
a) background asthenosphere, upper mantle slabs only



b) weak asthenosphere



c) weak layer within asthenosphere



d) subducted weak layer

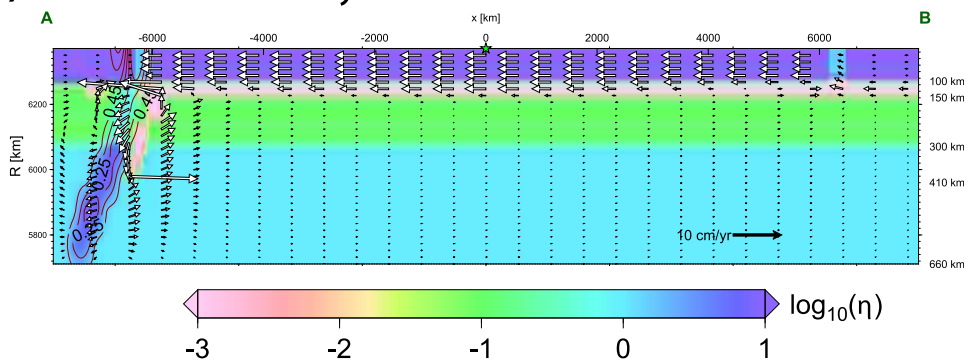


Figure 5. Cross-Pacific, upper mantle profiles using only upper mantle slabs to drive flow, else plot type and cross-section identical to Figures 4c–4e, see there for details.

underneath the Pacific (i.e., Couette-dominated flow) and some return flow at the base of the lower viscosity layer, as expected. Absolute surface velocities for those global flow models are too small compared to actual plate motions (Figure 2a). Those could be adjusted [Becker and O’Connell, 2001; Conrad and Lithgow-Bertelloni, 2002; Alisc et al., 2012]. However, here, I am mainly concerned with the relative velocities with depth, and hence the resulting shear, for the formation of anisotropy, and the overall contributions of slabs and other density anomalies for the upper mantle.

Allowing for a further asthenospheric viscosity reduction for the slab-only case (Figure 5b) increases the effect of the return flow close to the subducting slab in a way that is similar to what was discussed by *Nagef et al.* [2008]. Comparing Figures 4c and 5b illustrates that the disruption of anisotropic patterns seen in Figure 2f and 3 is due to a combination of density anomalies driving vertical flow (such as around Hawaii), and slab-induced, deep asthenosphere return flow as seen in Figure 5b. Therefore, even if the scaling that has been applied to the tomographic anomalies were to overestimate the role of buoyancy anomalies, I still expect the superweak asthenosphere to disrupt flow.

In map view (not shown), the slab/return flow component for an extremely weak asthenosphere leads to misalignment between predicted and observed anisotropy, for example in the NW Pacific. As was the case for the tomography-included computation, a thinner asthenospheric layer leads to shallower focusing of shear for the slab-only case (Figure 5c). In contrast, deep upper mantle, slab associated return is more broadly distributed with depth. Allowing for the subduction of weak asthenospheric material (Figure 5d) leads to broadly similar patterns, but a more symmetric transition between return flow, plate shearing, and return flow within the thin asthenosphere underneath the Pacific, from ridge to trench.

While the profiles shown in Figures 4 and 5 are for a single location only, comparison of Figures 2d and 2f suggests that the dynamics work out similarly for a large fraction of the suboceanic asthenosphere, in particular where flow is Couette-dominated, e.g., underneath the relatively fast-moving Pacific, Nazca, Indo-Australian plates. Local exceptions to this general behavior include the southern Atlantic domain where a superweak asthenosphere actually improves the fit to azimuthal anisotropy offshore Brazil. Analysis of velocity profiles for the region shows that this is due to flow confinement caused by the cratonic keels bounding the sub-Atlantic domain (cf., Figure 1). A relatively weaker asthenosphere allows for a more pronounced recirculation component of flow toward the spreading center underneath the South American plate, and this leads to a better fit than the broader Couette flow of the reference. This may indicate that the depth-extent or strength of the South American keel is underestimated in our reference model, for example.

3.3. Systematic Dependence on Asthenospheric Viscosity

Figure 6 explores the effects of a 200 km and 50 km wide, suboceanic asthenosphere systematically for three different azimuthally-anisotropic seismic tomography models. For the wide asthenosphere and my preferred flow model that includes upper mantle slabs and tomographic anomalies (Figure 6a), a notably clear signature of the asthenospheric background viscosity, η_a , arises. The lowest misfit to all three tomographic models considered, as well as the best match to plate motions, arises for $\eta_a \approx 0.1$. If I use the depth-averaged mean misfit instead of the minimum as in Figure 6, the dependence on η_a is the same (cf., Figure 3).

These findings substantiate that there is an emerging, long-wavelength consistency between different seismological models of upper mantle, azimuthal anisotropy [*Becker et al.*, 2007; *Schaeffer et al.*, 2016]. Geodynamic models are able to capture and explain common patterns in anisotropy [*Becker et al.*, 2003; *Conrad and Behn*, 2010]. While geopotential fields, plate velocities, and seismic anisotropy have different sensitivities to components of the mantle convection system [*Becker et al.*, 2003; *Ghosh et al.*, 2010; *Forte et al.*, 2015] a broadly consistent physical model of the Earth's mantle can be constructed.

The thin asthenosphere dependence of misfit metrics on η_a (Figure 6c) is similar to what was seen for the wide case and, again, all three tomographic models show a consistent dependence on η_a in terms of misfit. However, the best-fit values for η_a are shifted to smaller values, $\approx 0.045\eta_0$ for anisotropy or $\approx 0.01\eta_0$ for plate velocity correlations. Such a behavior might be expected if there is a trade-off between layer thickness and viscosity such that a combination of both is the major control on the decorrelation of anisotropy due to the flow modifications discussed above.

Further tests with an even thinner, 25 km wide suboceanic plate asthenospheric layer are at the limit of my numerical resolution capabilities at present, as only very few elements are available to resolve shear layers in this case. However, results are consistent with those for the 50 km layer case, albeit at a slightly reduced best-fit η_a of 0.01 for anisotropy from SL2013SVA and DR2015 (0.1 for YB13SV). The plate velocity correlation is almost constant and comparable to the values in Figure 6c for the range of preferred viscosity reductions, $\eta_a \leq 0.01$. Should this trade-off between η_a and layer thickness continue, I would expect a

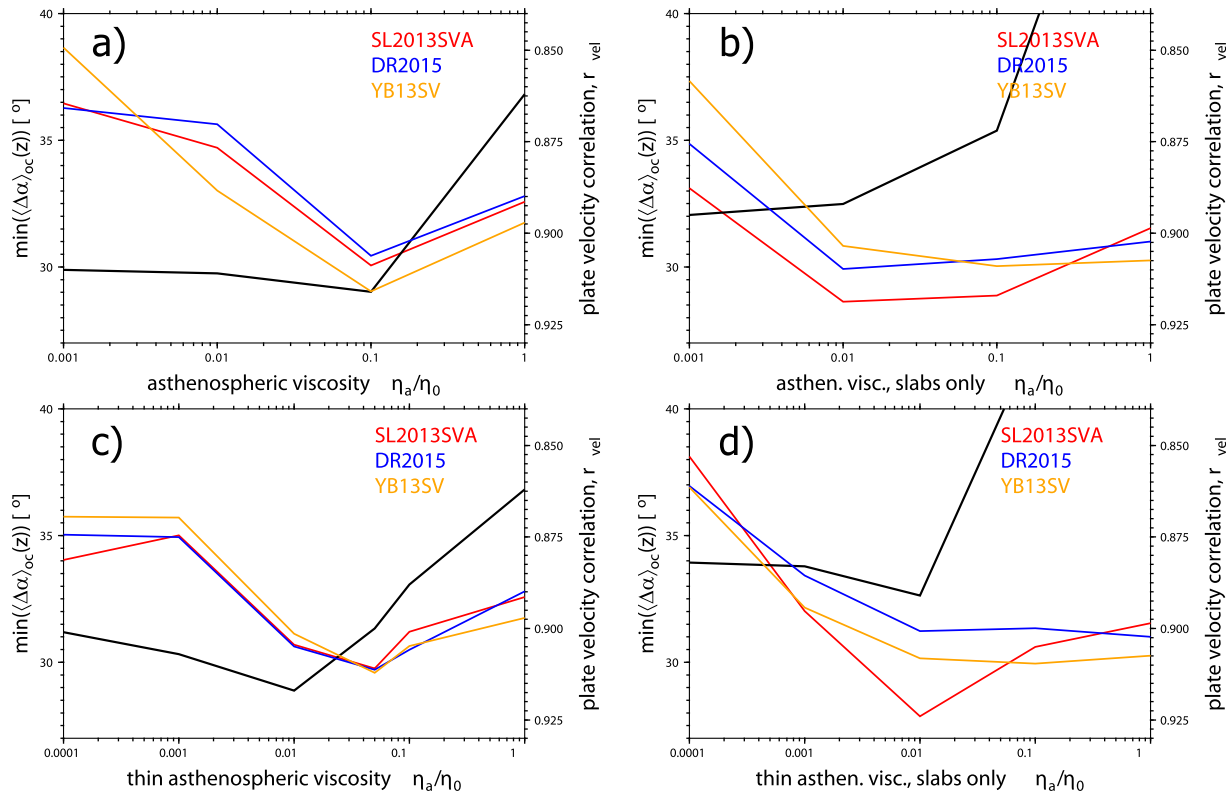


Figure 6. Minimum, mean angular misfit underneath oceanic plates with depth (cf. Figure 3; colored lines) and global plate velocity correlations (cf. Figure 2; black line) as a (a and b) function of 100–300 km asthenospheric viscosity and (c and d) 100–150 km asthenosphere for (a and c) models driven by slabs and tomography and (b and d) upper mantle slabs only. SL2013SVA, DR2015, and YB13SV are different seismic tomography models by *Schaeffer et al.* [2016], *Debayle and Ricard* [2013], and *Yuan and Beghein* [2013], respectively.

best-fit η_a of $\sim 0.002 \dots 0.005$ for a 5 km thickness asthenosphere or so. For the thinner layers, it is mainly the modification of the partitioning between Poiseuille and Couette flow that is affecting the match to anisotropy [cf., *Natarov and Conrad*, 2012], and not the vertical deflections of flow (cf., Figure 4).

While a broadly consistent viscosity reduction of $\eta_a \geq 0.01 \eta_0$ for thin asthenospheres (≥ 25 km) is found, azimuthal anisotropy misfit minima are thus predominantly sensitive to the bulk effect of layer thickness and viscosity. Comparison of Figures 3a and 3b shows that the reduction in the depth over which the asthenosphere is sheared for the thinner asthenosphere model leads to a slight depth-averaged degradation in overall model fit to tomography. This provides some indication that wider shear layers may be required to explain overall upper mantle anisotropy. However, radial anisotropy can be expected to provide a stronger constraint on the depth distribution of shear [*Becker et al.*, 2008]. For such an analysis, one would have to reevaluate the partitioning between dislocation and diffusion creep rheologies in light of LPO formation [*Podolefsky et al.*, 2004; *Becker*, 2006; *Behn et al.*, 2009], which is outside the scope here.

Figures 6b and 6d show results where I repeat the same tests for asthenospheric viscosity reduction for the slab-only model. The dependence of misfit to azimuthal anisotropy as a function of asthenospheric viscosity is less clear for the slab-induced shear component alone, but a preference for moderate viscosity reduction $0.01 \leq \eta_a/\eta_0 \leq 0.1$ is seen for the wide asthenosphere tests. Plate motions are expectedly not as well matched as for the tomography-included reference model, and the slab-only models are mainly meant to illustrate which flow component contributes how to the misfit degradation, as mentioned. That said, plate velocities correlations are still optimal for $\eta_a \approx 0.01$ but are less degraded at even smaller η_a , similar to the curves for the wide asthenosphere (Figure 6a).

I also repeated the tests for the thin suboceanic plate asthenosphere as in Figures 6c and 6d for an asthenosphere that gets dragged down behind the slab as shown in Figures 4e and 5d. The dependence of minimum azimuthal anisotropy misfit on η_a is very similar to the cases where the weak asthenospheric layer remains confined to the region underneath the plate only, for both tomography-included and slab only

cases. At least for my choices of implementing the asthenosphere, it is therefore not that important if the asthenosphere gets dragged down behind the slab or not. The general behavior can be captured by a wider asthenosphere underneath the oceanic plates that likewise facilitates the return flow close to the slab that is allowed by the subducted asthenosphere.

In summary, these tests indicate that a global, suboceanic asthenosphere is not only compatible but the preferred Earth model given the match to plate motions and seismic anisotropy, consistent with earlier work [Miller and Becker, 2012]. However, a global, contiguous layer cannot be too weak or else the fit to azimuthal anisotropy gets disrupted, and plate motion correlations are degraded for wide layers.

3.4. Superweak Patches

Figure 7 explores tests where I test the localized asthenospheric viscosity reduction models of Figures 2c–2f. As might be expected, the subduction zone (Figure 7a) or ridge and subduction zone (Figure 7b) low viscosity patches have very limited effects on the mean match to anisotropy or the fit to plate velocities (note zoom-in of misfit scales of Figure 7 compared to Figure 6). Low viscosity patches underneath the plates disrupt flow only locally and thus lead to a slight degradation of the match for all $\eta_a < 1$ tested. This does not mean that such local viscosity reductions do not exist, of course, and some of the deviations of asthenospheric anisotropy from expectations of plate-shear [e.g., Lin et al., 2016] or complexity of subduction zone anisotropy [e.g., Song and Kawakatsu, 2012; Long, 2013] may indeed be explained by local, superweak asthenosphere enhanced flow.

Moreover, some of the regional misfit between the reference model LPO predictions and anisotropic tomography (e.g., Figure 2d) may well be due to local asthenospheric viscosity variations underneath oceanic plates. For example, those may be due to partial melt or volatile variations (which may be linked, e.g., Ballmer et al. [2012]), and those are not captured by the temperature-dependence based on tomography assumed here besides the broad asthenospheric layering. While clearly a promising avenue for future work,

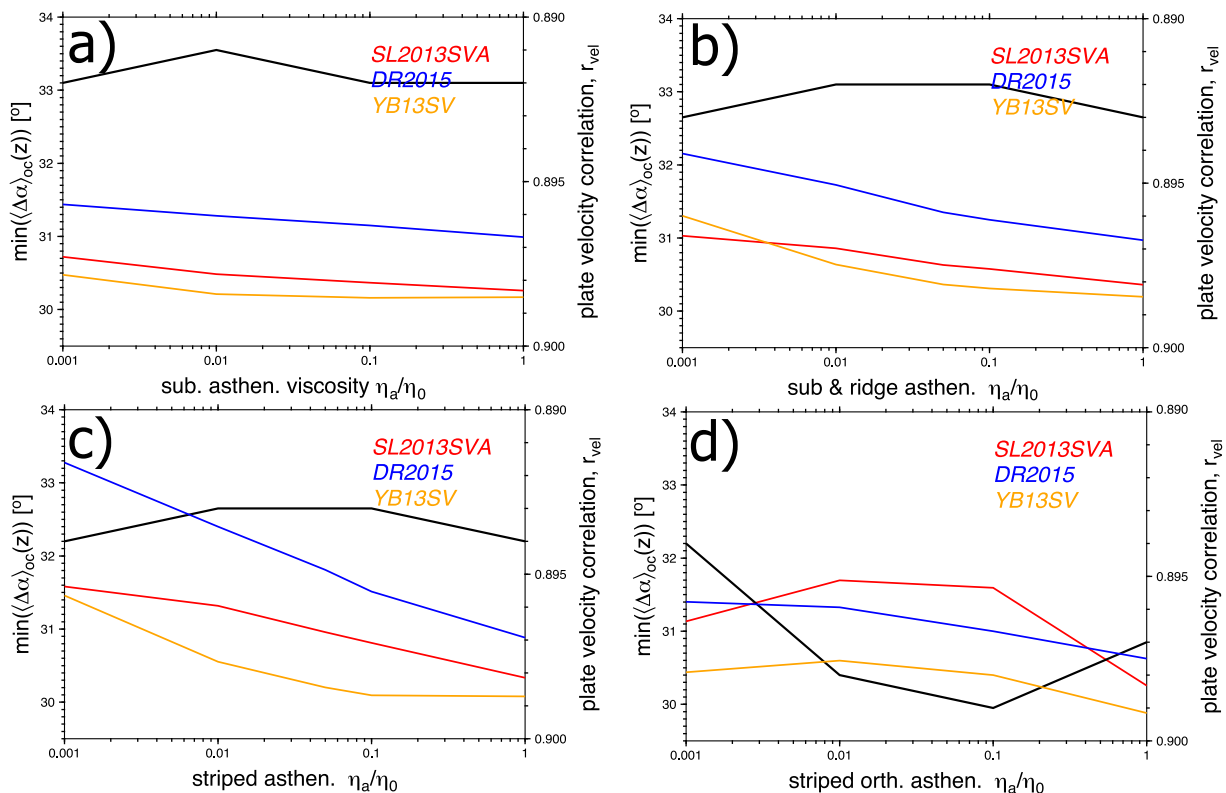


Figure 7. Minimum, mean angular misfit underneath oceanic plates with depth as in Figure 6, for models driven by tomography and upper mantle slabs, exploring localized viscosity reductions. Note that both azimuthal anisotropy and plate velocity misfit scales are adjusted compared to Figure 6 to highlight very small differences. The background viscosity of the asthenosphere between 100 and 300 km is 0.1 as in Figures 2c–2f. (a) Subduction zone weakness strip between 100 and 150 km (cf., Figure 2c); (b) subduction zone and ridge zones of weakness (Figure 2d); (c) striped zones of weakness (Figure 2e); and (d) orthogonal stripes (Figure 2f).

efforts of detecting local asthenospheric viscosity variations are likely contingent on a better understanding of the uncertainties of azimuthal anisotropy patterns from seismology and improved constraints on the types and conditions of LPO formation. For my purposes here, any such local viscosity reductions are expected to have only limited impact on global plate dynamics based on the tests conducted above.

When does local become regional or global? Increasing the number of low viscosity stripes to those shown in Figure 2e (Figure 7c) where the low viscosity patches cover $\approx 12\%$ of the Pacific plate, emphasizes this local disruption effect, leading to an overall decrease in mean angular fit of $\approx 3^\circ$. Such a difference is probably only borderline significant [Becker *et al.*, 2003], even though the misfit dependence on η_a is similar for all three seismological models considered. One can imagine that there is a continuum where further adding stripes of low viscosity beyond the case explored in Figure 7c will eventually reproduce the continuous layer results of Figure 6c. I will use $\geq 10\%$ areal coverage as the limit for global detectability of a superweak asthenosphere for the match to anisotropy, while plate velocities are still not significantly affected.

Last, Figure 7d shows results for the case where the low viscosity stripes are broadly aligned with the direction of shear and plate motions (Figure 2f) instead of orthogonal to it. The effect of η_a on the match to seismic anisotropy for this configuration is moderate, but the intermediate reduction in η_a around ~ 0.05 leads to a degradation of fit for all tomographic models. Plate velocities are overall improved compared to the other striped models, and prefer some moderate reduction of $\eta_a \sim 0.1$. While anisotropy is again not affected much in absolute terms, the signatures of anisotropy and plate velocities indicate a robust, but opposite and physically inconsistent, dependence on η_a . For mantle flow, the differences in trade-offs according to the alignment of asthenospheric stripes are similar to those between anisotropic and isotropic viscosity reduction in the asthenosphere under simple shear loading [Becker and Kawakatsu, 2011], as the effects of pure shear and pressure-driven flow are limited on plate scales (Figure 4).

4. Discussion

I showed that only a moderate bulk asthenosphere viscosity reduction appears consistent with the match of predicted flow and LPO anisotropy to observations. Most inferences were, however, based on variations of parameters starting off a reference model that was selected because it was doing fairly well in terms of matching the geoid and plate motions as well as regional anisotropy [Miller and Becker, 2012]. When inferring density anomalies from seismic tomography, for example, mantle velocity amplitudes will depend directly on the uncertain scaling of seismic velocity anomalies and density. Other combinations of mineral physics scalings and assumptions about compositional anomalies [e.g., Forte *et al.*, 2015] may potentially be consistent with different global asthenospheric viscosity reductions.

We might therefore be considering misleading tangents off one of several local misfit minima of the general inverse problem of inferring Earth dynamics. However, the slab-only models show that the circulation associated with plate motions, even without mantle density anomalies underneath the plates, is consistently affected such that an overly weak asthenosphere leads to a degradation of fit. Given these tests, and the relatively clear, physically plausible and general effect of changing η_a , I therefore doubt that my general conclusions would be affected strongly given different starting models.

Accepting the relative reduction of $\eta_a \geq 0.01$ relative to the upper mantle viscosity as a robust inference for a global, ≈ 200 km thick asthenosphere from modeling seismic anisotropy, this raises the question of consistency with other inferences on η_a . Predictions of upper mantle viscosity from laboratory derived creep laws are sensitive to uncertainties in the constants, in particular the activation volume, and local conditions such as volatile content and grain-size. However, variations of ~ 2 orders of magnitude between 100 km and 400 km depth appear broadly compatible with laboratory-based inferences [e.g., Hirth and Kohlstedt, 2004], as noted.

The "Haskell constraint" derived from postglacial rebound observations sets an absolute scale for the continental upper mantle; it indicates that the average viscosity of the upper ~ 1400 km should be $\approx 10^{21}$ Pas [Mitrovica, 1996]. Postseismic and postglacial deformation studies from continental regions have found local, asthenospheric viscosities that are significantly reduced compared to $\eta_0 \sim 10^{21}$ Pas. For example, Freed *et al.* [2006] infer values of $\sim 10^{18}$ Pas for the shallow mantle based on deformation after the 2002 Denali earthquake. Bills *et al.* [2007] suggest similar values for asthenospheric depths based on unloading of

Lake Lahontan, Nevada (though Bills et al.'s relatively weak mantle average appears to violate the Haskell constraint).

Given the vastly different time scales of loading from $\sim\mathcal{O}(10\text{ yr})$ for earthquakes, to $\sim\mathcal{O}(10,000\text{ yr})$ for postglacial adjustment, and $\sim\mathcal{O}(1\text{ Myr})$ in the case of mantle-flow induced anisotropy, different microscopic deformation mechanisms and/or transient rheologies may be at work [e.g., Bürgmann and Dresen, 2008]. However, the regional setting may also play a role, and we would expect locally reduced viscosities, e.g., due to enhanced partial melt fractions, in a mantle wedge atop a subducting slab or the tectonically active western United States where Farallon slab hydration has been suggested.

There are few geodetic studies constraining the asthenosphere underneath oceanic plates. Freed et al. [2017] find $\sim 10^{19}$ Pas for the asthenosphere below 100 km but had limited resolution there. A stronger constraint comes from the analysis of Hu et al. [2016] of deformation after the 2012 Indian Ocean earthquake. Using an upper mantle reference of 10^{20} Pas, the authors document a best-fit model trade-off between thickness and asthenospheric viscosity, with η_a between $\sim 0.5 \cdot 10^{18}$ Pas and 10^{19} Pas. In terms of absolute values, this would be only borderline consistent with our inference based on a ~ 0.01 reduction of $\eta_0 = 10^{21}$ Pas. However, absolute viscosity values for circulation computations are less well constrained than relative variations, and the relative reduction between Hu et al.'s best-fit asthenosphere and upper mantle viscosities is entirely consistent with my range of 0.01–0.1, depending on thickness.

This indicates at least the potential to reconcile short-term, geodetically constrained and long-term, mantle flow inferred viscosities for the asthenosphere underneath oceanic plates. The inferred relative drop of ~ 2 orders of magnitude from the upper mantle background is consistent, albeit possibly at smaller absolute values for the shorter timescale transients. Besides the role of temperature and pressure, no further partial melt or hydration effects need to be invoked in general, but those may well be the cause of patches of limited geographic extent that show further viscosity reduction.

I focused on the suboceanic domains, but my result that patchy viscosity reduction has limited impact on global plate dynamics is of relevance for the continental lithosphere as well. For example, Gung et al. [2003] suggested that strong continental keels may lead to shear localization and strong radial anisotropy underneath. Miller and Becker [2012] found that a better match to seismic anisotropy was achieved when the asthenospheric viscosity reduction in circulation models was limited to younger regions outside cratonic keels. Effects such as high melt content may well lubricate the lithosphere locally in tectonically active regions such as the western United States, outside old continental interiors, and only in limited regions. This would be consistent with the finding of Hopper and Fischer [2015], for example, that thermal effects alone may indeed explain the impedance contrast used to define the lithosphere-asthenosphere boundary below cratonic lithosphere, and that possible melt effects may not be laterally continuous.

Acknowledgments

I thank the editor, Janne Blichert-Toft, associate editor, Adrian Lenardic, and an anonymous reviewer for their comments which helped clarify and expand the discussion that is presented here. I also thank the original authors and CIG (geodynamics.org) for providing CitcomS, seismologists who share their tomographic models in electronic form, and Karen Fischer and Clint Conrad for helpful comments. All plots were made with the Generic Mapping Tools [Wessel and Smith, 1998]. I acknowledge the Texas Advanced Computing Center (TACC) at The University of Texas at Austin for providing high performance computing resources, and the National Science Foundation for partial support through NSF EAR 1460479. All input files and structural models used for this study are available upon request, and the CitcomS software used is available from and archived at CIG.

5. Conclusions

Seismic anisotropy and plate velocities indicate that there is a global, suboceanic plate asthenosphere which has a viscosity that is somewhere between 1/10 and 1/100 the viscosity of the upper mantle but not much weaker. This substantiates earlier work [e.g., Conrad and Behn, 2010; Miller and Becker, 2012] but is here explored with fully dynamically consistent flow models, and compared to three recent seismic tomography models, for the first time. Further, local viscosity reduction in isolated patches does not significantly affect global plate motions or the large-scale fit to anisotropy. This implies that even if features such as the recently imaged strong impedance contrasts at the base of lithospheric plates were indicative of rheological weakening, the global plate system would be mainly unaffected. In particular, a melt-induced viscosity reduction leading to a thin, weak layer would be compatible with global models of plate tectonics, as long as these patches remain discontinuous and have a total areal fraction of $\lesssim 10\%$ of the plate size.

References

- Alisc, L., M. Gurnis, G. Stadler, C. Burstedde, and O. Ghattas (2012), Multi-scale dynamics and rheology of mantle flow with plates, *J. Geophys. Res.*, *117*, B10402, doi:10.1029/2012JB009234.
- Auer, L., T. W. Becker, L. Boschi, and N. Schmerr (2015), Thermal structure, radial anisotropy, and dynamics of oceanic boundary layers, *Geophys. Res. Lett.*, *42*, 9740–9742, doi:10.1002/2015GL066246.

- Ballmer, M. D., C. P. Conrad, E. I. Smith, and N. Harmon (2012), Non-hotspot volcano chains produced by migration of shear-driven upwelling toward the East Pacific Rise, *Geology*, *41*, 479–482.
- Becker, T. W. (2006), On the effect of temperature and strain-rate dependent viscosity on global mantle flow, net rotation, and plate-driving forces, *Geophys. J. Int.*, *167*, 943–957.
- Becker, T. W. (2008), Azimuthal seismic anisotropy constrains net rotation of the lithosphere, *Geophys. Res. Lett.*, *35*, L05303, doi:10.1029/2007GL032928, correction: doi:10.1029/2008GL033946.
- Becker, T. W., and H. Kawakatsu (2011), On the role of anisotropic viscosity for plate-scale flow, *Geophys. Res. Lett.*, *38*, L17307, doi:10.1029/2011GL048584.
- Becker, T. W., and R. J. O'Connell (2001), Predicting plate velocities with geodynamic models, *Geochem. Geophys. Geosyst.*, *2*, 1060, doi:10.1029/2001GC000171.
- Becker, T. W., J. B. Kellogg, G. Ekström, and R. J. O'Connell (2003), Comparison of azimuthal seismic anisotropy from surface waves and finite-strain from global mantle-circulation models, *Geophys. J. Int.*, *155*, 696–714.
- Becker, T. W., S. Chevrot, V. Schulte-Pelkum, and D. K. Blackman (2006), Statistical properties of seismic anisotropy predicted by upper mantle geodynamic models, *J. Geophys. Res.*, *111*, B08309, doi:10.1029/2005JB004095.
- Becker, T. W., G. Ekström, L. Boschi, and J. W. Woodhouse (2007), Length-scales, patterns, and origin of azimuthal seismic anisotropy in the upper mantle as mapped by Rayleigh waves, *Geophys. J. Int.*, *171*, 451–462.
- Becker, T. W., B. Kustowski, and G. Ekström (2008), Radial seismic anisotropy as a constraint for upper mantle rheology, *Earth Planet. Sci. Lett.*, *267*, 213–237.
- Becker, T. W., C. P. Conrad, A. J. Schaeffer, and S. Lebedev (2014), Origin of azimuthal seismic anisotropy in oceanic plates and mantle, *Earth Planet. Sci. Lett.*, *401*, 236–250.
- Beghein, C., K. Yuan, N. Schmerr, and Z. Xing (2014), Changes in seismic anisotropy shed light on the nature of the Gutenberg discontinuity, *Science*, *343*(6176), 1237–1240, doi:10.1126/science.1246724.
- Behn, M. D., C. P. Conrad, and P. G. Silver (2004), Detection of upper mantle flow associated with the African Superplume, *Earth Planet. Sci. Lett.*, *224*, 259–274.
- Behn, M. D., G. Hirth, and J. R. Elsenbeck II (2009), Implications of grain size evolution on the seismic structure of the oceanic upper mantle, *Earth Planet. Sci. Lett.*, *282*, 178–189.
- Billen, M. I., and G. Hirth (2005), Newtonian versus non-Newtonian upper mantle viscosity: Implications for subduction initiation, *Geophys. Res. Lett.*, *32*, L19304, doi:10.1029/2005GL023457.
- Bills, B., K. D. Adams, and S. G. Wesnousky (2007), Viscosity structure of the crust and upper mantle in western Nevada from isostatic rebound patterns of the late Pleistocene Lake Lahontan high shoreline, *J. Geophys. Res.*, *112*, B06405, doi:10.1029/2005JB003941.
- Buffett, B., and T. W. Becker (2012), Bending stress and dissipation in subducted lithosphere, *J. Geophys. Res.*, *117*, B05413, doi:10.1029/2012JB009205.
- Bürgmann, R., and G. Dresen (2008), Rheology of the lower crust and upper mantle: Evidence from rock mechanics, geodesy, and field observations, *Annu. Rev. Earth Planet. Sci.*, *36*, 531–567.
- Burgos, G., J.-P. Montagner, E. Beucler, Y. Capdeville, A. Mocquet, and M. Drilleau (2014), Oceanic lithosphere/asthenosphere boundary from surface wave dispersion data, *J. Geophys. Res. Solid Earth*, *119*, 1079–1093, doi:10.1002/2013JB010528.
- Castelnau, O., D. K. Blackman, and T. W. Becker (2009), Numerical simulations of texture development and associated rheological anisotropy in regions of complex mantle flow, *Geophys. Res. Lett.*, *36*, L12304, doi:10.1029/2009GL038027.
- Conrad, C. P., and M. Behn (2010), Constraints on lithosphere net rotation and asthenospheric viscosity from global mantle flow models and seismic anisotropy, *Geochem. Geophys. Geosyst.*, *11*, Q05W05, doi:10.1029/2009GC002970.
- Conrad, C. P., and C. Lithgow-Bertelloni (2002), How mantle slabs drive plate tectonics, *Science*, *298*, 207–209.
- Debayle, E., and Y. Ricard (2013), Seismic observations of large-scale deformation at the bottom of fast-moving plates, *Earth Planet. Sci. Lett.*, *376*, 165–177.
- DeMets, C., R. G. Gordon, D. F. Argus, and S. Stein (1994), Effect of recent revisions to the geomagnetic reversal time scale on estimates of current plate motions, *Geophys. Res. Lett.*, *21*, 2191–2194.
- Foley, B., and T. W. Becker (2009), Generation of plate tectonics and mantle heterogeneity from a spherical, viscoplastic convection model, *Geochem. Geophys. Geosyst.*, *10*, Q08001, doi:10.1029/2009GC002378.
- Forsyth, D. W., and S. Uyeda (1975), On the relative importance of the driving forces of plate motion, *Geophys. J. R. Astron. Soc.*, *43*, 163–200.
- Forte, A. M., N. A. Simons, and S. P. Grand (2015), Constraints on seismic models from other disciplines - Constraints on 3-D seismic models from global geodynamic observables: Implications for the global mantle convective flow, in *Treatise on Geophysics*, 2nd ed., vol. 1, edited by G. Schubert, pp. 853–907, Elsevier, Oxford.
- Freed, A. M., R. Bürgmann, E. Calais, J. Freymueller, and S. Hreinsdóttir (2006), Implications of deformation following the 2002 Denali, Alaska earthquake for postseismic relaxation processes and lithospheric rheology, *J. Geophys. Res.*, *111*, B01401, doi:10.1029/2005JB003894.
- Freed, A., A. Hashima, T. W. Becker, D. A. Okaya, H. Sato, and Y. Hatanaka (2017), Resolving depth-dependent subduction zone viscosity and afterslip from postseismic displacements following the 2011 Tohoku-oki, Japan earthquake, *Earth Planet. Sci. Lett.*, *459*, 279–290.
- Gaboret, C., A. M. Forte, and J.-P. Montagner (2003), The unique dynamics of the Pacific Hemisphere mantle and its signature on seismic anisotropy, *Earth Planet. Sci. Lett.*, *208*, 219–233.
- Ghosh, A., T. W. Becker, and S. Zhong (2010), Effects of lateral viscosity variations on the geoid, *Geophys. Res. Lett.*, *37*, L01301, doi:10.1029/2009GL040426.
- Gudmundsson, O., and M. Sambridge (1998), A regionalized upper mantle (RUM) seismic model, *J. Geophys. Res.*, *103*, 7121–7136.
- Gung, Y., M. Panning, and B. Romanowicz (2003), Global anisotropy and the thickness of continents, *Nature*, *422*, 707–711.
- Gurnis, M., and G. F. Davies (1986), The effect of depth-dependent viscosity on convective mixing in the mantle and the possible survival of primitive mantle, *Geophys. Res. Lett.*, *13*, 541–544.
- Gutenberg, B. (1959), The asthenosphere low-velocity layer, *Ann. Geophys.*, *12*, 439–460.
- Hager, B. H. (1984), Subducted slabs and the geoid: Constraints on mantle rheology and flow, *J. Geophys. Res.*, *89*, 6003–6015.
- Hager, B. H., and R. J. O'Connell (1981), A simple global model of plate dynamics and mantle convection, *J. Geophys. Res.*, *86*, 4843–4867.
- Hansen, L. N., C. Qib, and J. M. Warren (2016), Olivine anisotropy suggests Gutenberg discontinuity is not the base of the lithosphere, *Proc. Natl. Acad. Sci. U. S. A.*, *113*, 10,503–10,506.
- Hawley, W. B., R. Allen, and M. A. Richards (2016), Tomography reveals buoyant asthenosphere accumulating beneath the Juan de Fuca plate, *Science*, *353*, 1406–1408.
- Hirschmann, M. M. (2010), Partial melt in the oceanic low velocity zone, *Phys. Earth Planet. Inter.*, *179*, 60–71.

- Hirth, G., and D. L. Kohlstedt (2004), Rheology of the upper mantle and the mantle wedge: A view from the experimentalists, in *Inside the Subduction Factory*, *Geophys. Monogr.*, vol. 138, edited by J. Eiler, pp. 83–105, AGU, Washington, D. C.
- Hoink, T., and A. Lenardic (2008), Three-dimensional mantle convection simulations with a low viscosity asthenosphere and the relationship between heat flow and the horizontal length scale of convection, *Geophys. Res. Lett.*, *35*, L10304, doi:10.1029/2008GL033854.
- Hoink, T., and A. Lenardic (2010), Long wavelength convection, Poiseuille-Couette flow in the low-viscosity asthenosphere and the strength of plate margins, *Geophys. J. Int.*, *180*, 23–33.
- Holtzman, B. (2016), Questions on the existence, persistence, and mechanical effects of a very small melt fraction in the asthenosphere, *Geochem. Geophys. Geosyst.*, *17*, 470–484, doi:10.1002/2015GC006102.
- Hopper, E., and K. M. Fischer (2015), The meaning of midlithospheric discontinuities: A case study in the northern U.S. craton, *Geochem. Geophys. Geosyst.*, *16*, 4057–4083, doi:10.1002/2015GC006030.
- Hu, Y., R. Bürgmann, P. Banerjee, L. Feng, E. M. Hill, T. Ito, T. Tabei, and K. Wang (2016), Asthenosphere rheology inferred from observations of the 2012 Indian Ocean earthquake, *Nature*, *538*, 368–372.
- Jarvis, G. T., and W. R. Peltier (1989), Convection models and geophysical observations, in *Mantle convection: Plate Tectonics and Global Dynamics*, *The Fluid Mechanics of Astrophysics and Geophysics*, vol. 4, edited by W. R. Peltier, pp. 479–593, Gordon and Breach, New York.
- Jeanloz, R., and S. Morris (1987), Is the mantle geotherm sub-adiabatic?, *Geophys. Res. Lett.*, *14*, 335–338.
- Kaminski, É., N. M. Ribe, and J. T. Browaeys (2004), D-Rex, a program for calculation of seismic anisotropy due to crystal lattice preferred orientation in the convective upper mantle, *Geophys. J. Int.*, *157*, 1–9.
- Kawakatsu, H., P. Kumar, Y. Takei, M. Shinohara, T. Kanazawa, E. Araki, and K. Suyehiro (2009), Seismic evidence for sharp lithosphere-asthenosphere boundaries of oceanic plates, *Science*, *324*, 499–502.
- King, S. D. (1995), Radial models of mantle viscosity: Results from a genetic algorithm, *Geophys. J. Int.*, *122*, 725–734.
- Lenardic, A., M. A. Richards, and F. H. Busse (2006), Depth-dependent rheology and the horizontal length-scale of mantle convection, *J. Geophys. Res.*, *111*, B07404, doi:10.1029/2005JB003639.
- Lin, P.-Y. P., J. B. Gaherty, J. G., J. A. Collins, D. Lizarralde, R. L. Evans, and G. Hirth (2016), High-resolution seismic constraints on flow dynamics in the oceanic asthenosphere, *Nature*, *535*, 538–541.
- Liu, L., and Q. Zhou (2015), Deep recycling of oceanic asthenosphere material during subduction, *Geophys. Res. Lett.*, *42*, 2204–2211, doi:10.1002/2015GL063633.
- Long, M. D. (2013), Constraints on subduction geodynamics from seismic anisotropy, *Rev. Geophys.*, *51*, 76–112, doi:10.1002/rog.20008.
- Long, M. D., and T. W. Becker (2010), Mantle dynamics and seismic anisotropy, *Earth Planet. Sci. Lett.*, *297*, 341–354.
- McKenzie, D. P. (1979), Finite deformation during fluid flow, *Geophys. J. R. Astron. Soc.*, *58*, 689–715.
- Miller, M. S., and T. W. Becker (2012), Mantle flow deflected by interactions between subducted slabs and cratonic keels, *Nat. Geosci.*, *5*, 726–730.
- Mitrovica, J. X. (1996), Haskell [1935] revisited, *J. Geophys. Res.*, *101*, 555–569.
- Mitrovica, J. X., and A. M. Forte (2004), A new inference of mantle viscosity based upon joint inversion of convection and glacial isostatic adjustment data, *Earth Planet. Sci. Lett.*, *225*, 177–189.
- Montagner, J.-P., and T. Tanimoto (1991), Global upper mantle tomography of seismic velocities and anisotropies, *J. Geophys. Res.*, *96*, 20,337–20,351.
- Moresi, L. N., and V. S. Solomatov (1995), Numerical investigations of 2D convection with extremely large viscosity variations, *Phys. Fluids*, *7*, 2154–2162.
- Nagel, T. J., W. B. F. Ryan, A. Malinverno, and W. R. Buck (2008), Pacific trench motions controlled by the asymmetric plate configuration, *Tectonics*, *27*, TC3005, doi:10.1029/2007TC002183.
- Naif, S., K. Key, S. Constable, and R. L. Evans (2013), Melt-rich channel observed at the lithosphere-asthenosphere boundary, *Nature*, *495*, 356–359.
- Natarov, S. I., and C. P. Conrad (2012), The role of Poiseuille flow in creating depth-variation of asthenospheric shear, *Geophys. J. Int.*, *190*, 1297–1310.
- Olson, P. (1981), Mantle convection with spherical effects, *J. Geophys. Res.*, *86*, 4881–4890.
- Panasjuk, S. V., and B. H. Hager (2000), Models of isostatic and dynamic topography, geoid anomalies, and their uncertainties, *J. Geophys. Res.*, *105*, 28,199–28,209.
- Paulson, A., S. Zhong, and J. Wahr (2005), Modelling post-glacial rebound with lateral viscosity variations, *Geophys. J. Int.*, *163*, 357–371.
- Phipps Morgan, J., W. J. Morgan, Y.-S. Zhang, and W. H. F. Smith (1995), Observational hints for a plume-fed, suboceanic asthenosphere and its role in mantle convection, *J. Geophys. Res.*, *100*, 12,753–12,767.
- Podolefsky, N. S., S. Zhong, and A. K. McNamara (2004), The anisotropic and rheological structure of the oceanic upper mantle from a simple model of plate shear, *Geophys. J. Int.*, *158*, 287–296.
- Ricard, Y., and C. Vigny (1989), Mantle dynamics with induced plate tectonics, *J. Geophys. Res.*, *94*, 17,543–17,559.
- Ricard, Y., C. Doglioni, and R. Sabadini (1991), Differential rotation between lithosphere and mantle: A consequence of lateral mantle viscosity variations, *J. Geophys. Res.*, *96*, 8407–8415.
- Richards, M., W.-S. Yang, J. Baumgardner, and H.-P. Bunge (2001), Role of a low-viscosity zone in stabilizing plate tectonics: Implications for comparative terrestrial planetology, *Geochem. Geophys. Geosyst.*, *2*, 1026, doi:10.1029/2000GC000115.
- Richter, F. M. (1973), Convection and the large-scale circulation of the mantle, *J. Geophys. Res.*, *78*, 8735–8745.
- Schaeffer, A., S. Lebedev, and T. W. Becker (2016), Azimuthal seismic anisotropy in the Earth's upper mantle and the thickness of tectonic plates, *Geophys. J. Int.*, *207*, 901–933.
- Silver, P. G. (1996), Seismic anisotropy beneath the continents: Probing the depths of geology, *Annu. Rev. Earth Planet. Sci.*, *24*, 385–432.
- Song, T.-R. A., and H. Kawakatsu (2012), Subduction of oceanic asthenosphere: Evidence from sub-slab seismic anisotropy, *Geophys. Res. Lett.*, *39*, L17301, doi:10.1029/2012GL052639.
- Stern, T. A., S. A. Henrys, D. Okaya, J. N. Louie, M. K. Savage, S. Lamb, H. Sato, R. Sutherland, and T. Iwasak (2015), A seismic reflection image for the base of a tectonic plate, *Nature*, *518*, 85–88.
- Stixrude, L., and C. Lithgow-Bertelloni (2005), Mineralogy and elasticity of the upper mantle: Origin of the low velocity zone, *J. Geophys. Res.*, *110*, B03204, doi:10.1029/2004JB002965.
- Tackley, P. J. (2000), Self-consistent generation of tectonic plates in time-dependent, three-dimensional mantle convection simulations. 2. Strain weakening and asthenosphere, *Geochem. Geophys. Geosyst.*, *1*, 1026, doi:10.1029/2000GC000043.
- Tanimoto, T., and D. L. Anderson (1984), Mapping convection in the mantle, *Geophys. Res. Lett.*, *11*, 287–290.
- van Heck, H., and P. J. Tackley (2008), Planforms of self-consistently generated plate tectonics in 3-D spherical geometry, *Geophys. Res. Lett.*, *35*, L19312, doi:10.1029/2008GL035190.

- van Summeren, J., C. P. Conrad, and C. Lithgow-Bertelloni (2012), The importance of slab pull and a global asthenosphere to plate motions, *Geochem. Geophys. Geosyst.*, *13*, Q0AK03, doi:10.1029/2011GC003873.
- Walker, K. T., G. H. R. Bokelmann, S. L. Klemperer, and A. Nyblade (2005), Shear-wave splitting around hotspots: Evidence for upwelling-related mantle flow?, in *Plates, Plumes, and Paradigms*, *Geol. Soc. Am. Spec. Pap.*, vol. 388, edited by G. Foulger et al., pp. 171–192, *Geol. Soc. Am.*, doi: 10.1130/2005.2388(11).
- Wessel, P., and W. H. F. Smith (1998), New, improved version of the Generic Mapping Tools released, *Eos Trans. AGU*, *79*, 579.
- Yuan, K., and C. Beghein (2013), Seismic anisotropy changes across upper mantle phase transitions, *Earth Planet. Sci. Lett.*, *374*, 132–144.
- Zhong, S. (2001), Role of ocean-continent contrast and continental keels on plate motion, net rotation of lithosphere, and the geoid, *J. Geophys. Res.*, *106*, 703–712.
- Zhong, S., M. T. Zuber, L. N. Moresi, and M. Gurnis (2000), Role of temperature-dependent viscosity and surface plates in spherical shell models of mantle convection, *J. Geophys. Res.*, *105*, 11,063–11,082.